Laser and Particle Beams (2017), *35*, 126–136.

doi:10.1017/S0263034616000914

Defects in quantum ring to control high-harmonic spectrum

E. FIORDILINO AND B. FRUSTERI

Dipartimento di Fisica e Chimica, Università degli Studi Palermo, Via Archirafi 36, 90123, Palermo, Italy

(RECEIVED 5 October 2016; ACCEPTED 15 December 2016)

Abstract

The high-harmonic generation from a structured quantum ring (SQR) driven by an intense laser field is presented within the single active electron approximation. The spectrum is studied by varying the symmetry of the physical system. The standard SQR (six identical and equidistant dots in a ring) presents a 60° rotational symmetry, that in this work is broken, moving or changing only one potential hole. We find that careful designed breaking of the geometrical symmetry of the SQR opens the possibility of controlling the characteristics of the harmonic lines such as intensity and polarization. HHG analysis of the emission spectrum performed through a Morlet wavelet, shows that the high-frequency emission occurs during short time intervals.

Keywords: Electron dynamics; High-harmonic generation; Intense laser; Quantum ring; Time-resolved spectroscopy

1. INTRODUCTION: STRUCTURED NANORING WITH DEFECTS

A recent frontier of optics is the study of the interaction between strong laser pulses and low-dimensional nano-sized systems. Particular interesting structures are the artificial atoms or molecules, quantum confinement of only few electrons, named quantum dots (QDs). In the realization stage, QDs can be tailored almost at will to reproduce characteristics of systems such as atoms, nuclei, metallic clusters, trapped atomic gases, or to implement new desired features. For example, a way to set the electronic properties of a finite man-made low-dimensional system is by electrostatic gating (Kouwenhoven *et al.*, 2001; van Kouwen *et al.*, 2010), or by application of an external magnetic field. Thus, these artificial systems can be potentially employed for a large variety of purposes.

The aim of this paper is the investigation of the interaction between a strong laser field and nanorings (Wang, 2004; Guo *et al.*, 2008; Hoffmann *et al.*, 2008; Hinsche *et al.*, 2009; O'Sullivan *et al.*, 2011; Cricchio & Fiordilino, 2014, 2016): in particular we study a one-dimensional (1D) structured quantum ring (SQR) (Castiglia *et al.*, 2015), consisting of M point like QDs along an annular structure of radius R. Matter driven by a strong laser field of frequency ω_L emits electromagnetic radiation whose spectrum is formed by multiples of ω_L with a fast-decreasing emission in the first part of the spectrum, a broad plateau region until a cut-off frequency ω_M. This phenomenon is called high-harmonic generation (HHG) (L'Huillier *et al.*, 1991; Gavrila, 1992; Corkum, 1993; Lewenstein *et al.*, 1994; Zuo *et al.*, 1995; Alon *et al.*, 1998; Bâldea *et al.*, 2004; Xie *et al.*, 2008; Ozaki *et al.*, 2007, 2010; Ciappina *et al.*, 2008; Ganeev *et al.*, 2009, 2012; Zhukovsky, 2016). In atoms, HHG is generally explained by the three-step model, thus as an outcome of the ionization and recombination process. Nevertheless the origin of the emission resides in the electron acceleration, whatever its origin is; actually HHG can be obtained also from bound–bound as well as free–free transitions (Daniele & Fiordilino, 1996; Di Piazza & Fiordilino, 2001; Orlando *et al.*, 2008; Fiordilino *et al.*, 2017). Our model does not support ionization, since the active charges are bound along the ring thus the emission is caused by the electron acceleration maybe during violent collisions with the dots. Here, for simplicity sake, we confine ourselves to study the six-dot problem within the single active electron approximation that, in the HHG emission, is largely used (Schafer *et al.*, 1993; Bauer, 1997; Daniele *et al.*, 2009).

The HHG is very interesting from many points of view. Various experiments show that to obtain a cutoff of $\omega_M \approx 100\omega_L$ is possible, then HHG allows us to obtain emission in the far-UV or near-X-ray range from an incident laser in the visible region (Baer *et al.*, 2003; Brandi *et al.*, 2003; Chang, 2004; Eden, 2004; Ganeev *et al.*, 2005; Heinrich *et al.*, 2006). The coherent properties of the emitted light and the large plateau that, mainly for molecular systems, presents very close lines, allow technological and scientific

Address correspondence and reprint requests to: B. Frusteri, Dipartimento di Fisica e Chimica, Università degli Studi Palermo, Via Archirafi 36, 90123, Palermo, Italy. E-mail: biagio.frusteri@unipa.it

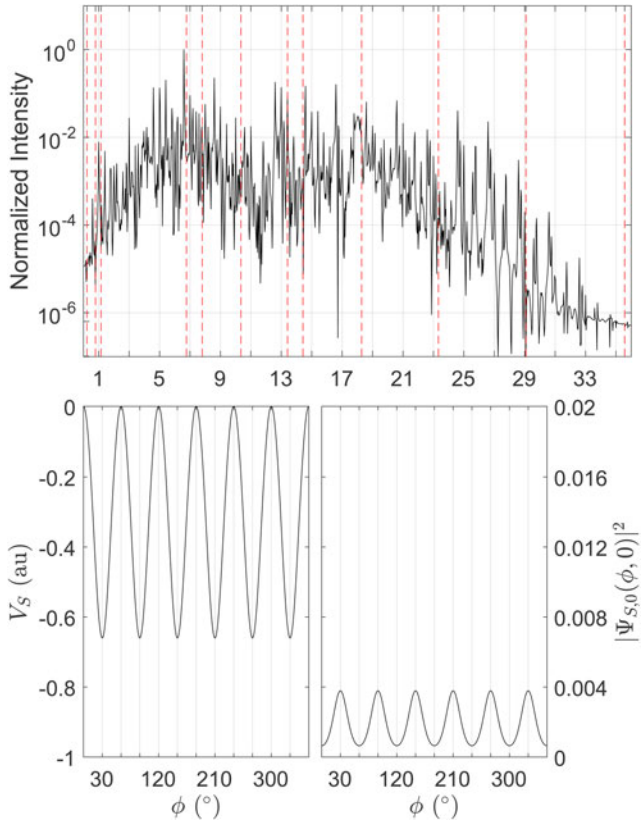

Fig. 1. First row: Fourier spectrum, vertical dashed red lines show energy differences between excited states and ground-state; second row: in the left side, V_S versus ϕ and in the right side, ground state square modulus versus ϕ. The values of the parameters are: $V_0 = 0.33$ au, $R = 5$ au, $\eta_1 = \eta_0 = 0.1333$, $K_1 = K_0 = 1.9420$ au, $\phi_i = 30°, 90°, 150°, 210°, 270°, 330°$, $\lambda = 780$ nm, $I_0 = 4 \cdot 10^{14}$W/cm^2, trapezoidal shape(32 oc, 3 up, and 3 down) linearly polarized with $\phi_L = 60°$. System with C6 symmetry.

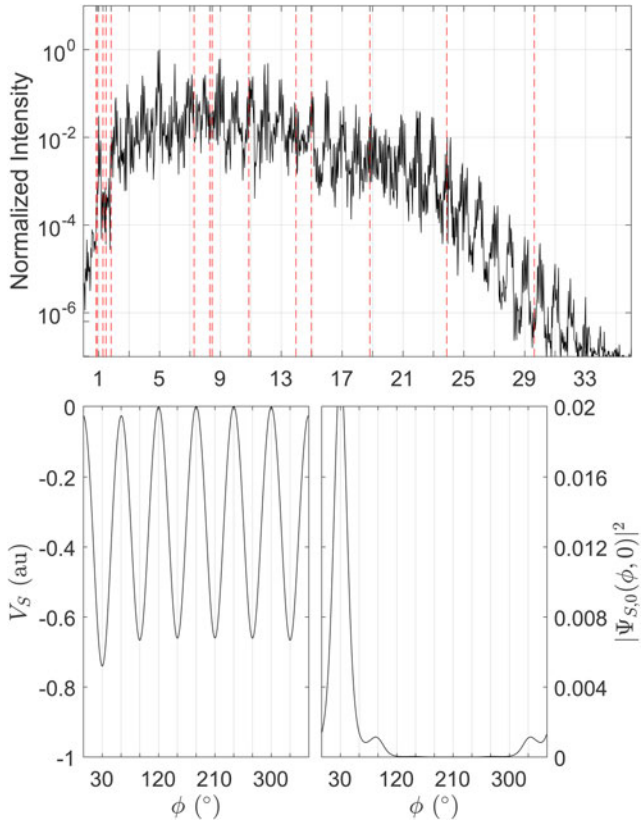

Fig. 2. Caption as Figure 1 but with $\eta_1 = 0.97\eta_0 = 0.1293$, which breaks the C6 symmetry.

improvement, such as generation of train of attosecond pulses or of a single isolate attosecond pulse and also the external seeding of free-electron lasers (Orlando *et al.*, 2009*a*, *b*; Allaria *et al.*, 2010; Crawford-Uranga *et al.*, 2014; Solanpää *et al.*, 2014).

In order to follow in detail the particle dynamics, the necessity of using new methods for producing extremely short light pulses emerges. The most efficient tool is the superposition of a clip of the spectrum emitted by a source, and the shortest possible pulse duration is given by the optical bandwidth $\Delta\omega$ of the radiation. Thus, to think that the HHG could be used in the ultrafast science is natural (Farkas & Tóth, 1992; Antoine *et al.*, 1996; Krausz & Ivanov, 2009). The main benefit of using HHG to make attosecond pulses, is that the presence of a large plateau allows the increase of the bandwidth $\Delta\omega$ with a subsequent reduction of the pulse duration $\tau \approx 1/(\Delta\omega)$. The principal problem in the use of HHG is the low efficiency of conversion of the energy from the laser to the emitted radiation, thus an eventually extremely short light pulse, made in this way, will be weak. For this reason phase-matching techniques are implemented to increase the efficiency (Rundquist *et al.*, 1998). Actually it is also demonstrated that although the plateau harmonics were not in phase, the single atom spectrum consists of a train of ultrashort pulses (Paul *et al.*, 2001; Lein, 2005; Zepf *et al.*, 2007; Orlando *et al.*, 2008; Strelkov, 2010).

It is well known that the internal symmetry of the matter during HHG strongly affects the emission process and the overall aspect of the spectrum such as plateau extension, yield, and presence of odd and even harmonics. Therefore, if control of the spectrum is looked for, the symmetry of the system provides a versatile knob for the purpose. Both atoms and molecules are very studied, and in particular molecules are sources of very rich HHG spectra, but their applications have been quite limited. For these reasons, the study of the emission by a system that can be easily fabricated such as the SQR can be very promising.

In literature (Castiglia *et al.*, 2015), the SQR is studied as a 1D system with identical and equidistant scattering centers with the potential energy experienced by the electron taken as:

$$\mathbb{V}_C(\phi) = V_0 \cos(M\phi). \tag{1}$$

In this paper, we consider a soft-core potential energy:

$$\mathbb{V}_S(\phi) = \sum_{n=1}^{6} -\frac{K_n}{\sqrt{\eta_n + 1 - \cos(\phi - \phi_n)}} \tag{2}$$

https://doi.org/10.1017/S0263034616000914 Published online by Cambridge University Press

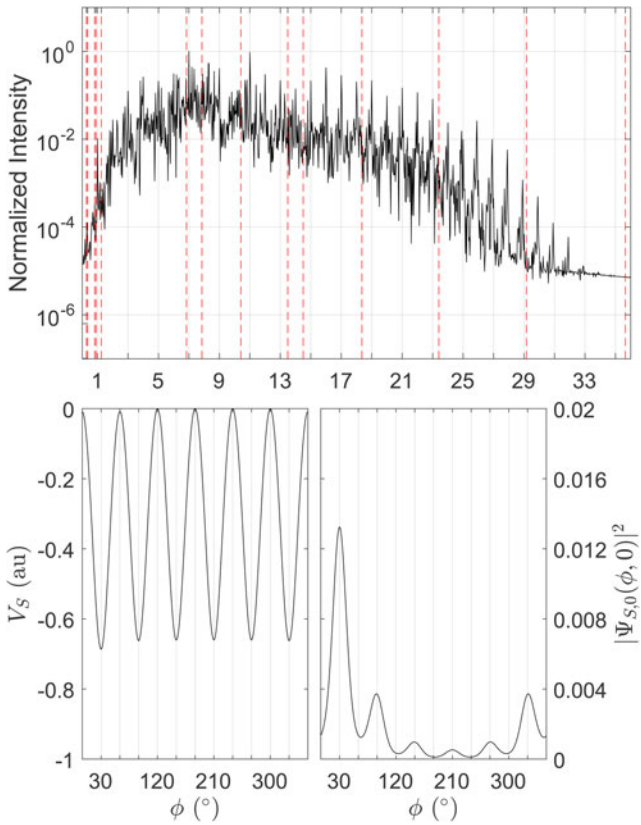

Fig. 3. Caption as Figure 1 but with $\eta_1 = 0.99\eta_0 = 0.1320$, which breaks the C6 symmetry.

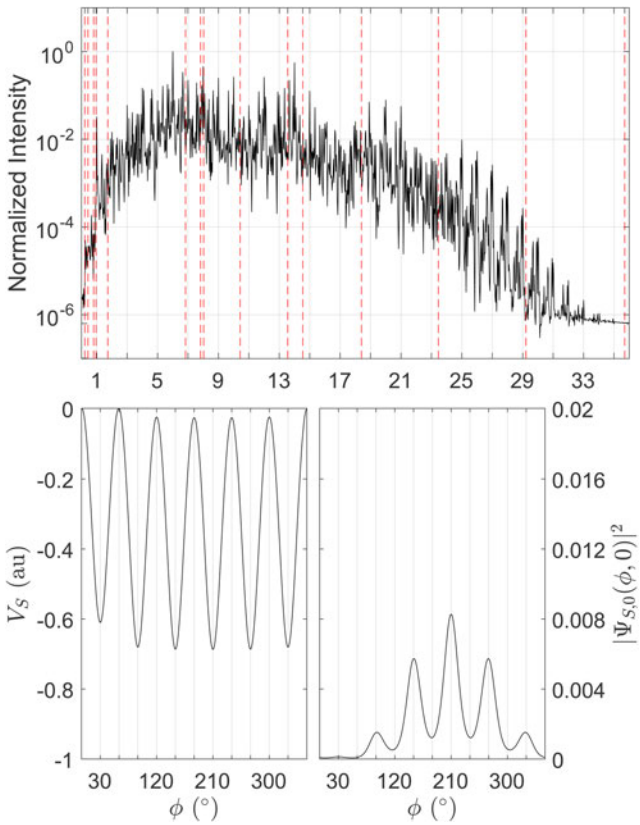

Fig. 4. Caption as Figure 1 but with $\eta_1 = 1.03\eta_0 = 0.1373$, which breaks the C6 symmetry.

that mimics the presence of $M = 6$ dots, not necessarily equal, at the angular position ϕ_n, where η_n are soft-core constants and K_n normalization constants. The need for writing the potential energy in this way comes from the requirement of introducing asymmetries to model defects of the system. For comparison sake, we start our calculations by considering the symmetrical case with $\eta_n = \eta_0$, $K_n = K_0$ and $\phi_n = -30° + n60°$. The constants in V_S must be chosen in such a way to get $|V_S(30°) - V_S(0°)| = 2V_0$. For $V_0 = 0.33$ au, by taking $K_0 = 1.9420$ au, and $\eta_0 = 2/15$ the solutions of the time-independent Schrödinger equations:

$$\mathbb{H}_T \Psi_{T,n}(\phi, 0) = E_{T,n} \Psi_{T,n}(\phi, 0), \tag{3}$$

$$\mathbb{H}_T = -\frac{\hbar^2}{2m_e R^2} \frac{\partial^2}{\partial \phi^2} + \mathbb{V}_T(\phi), \tag{4}$$

with $T = C, S$ give $E_{S,n} - E_{S,0} \cong E_{C,n} - E_{C,0}$.

2. THEORY

To evaluate the HHG spectrum, we solve the time-dependent Schrödinger equation in the dipole approximation:

$$i\hbar \frac{\partial}{\partial t} \Psi(\phi, t) = \mathbb{H} \Psi(\phi, t) \tag{5}$$

with Hamiltonian:

$$\mathbb{H} = \mathbb{H}_S - e\boldsymbol{r} \cdot \varepsilon, \tag{6}$$

$$\boldsymbol{r} \cdot \varepsilon = R\cos(\phi)\varepsilon_x + R\sin(\phi)\varepsilon_y, \tag{7}$$

and $\boldsymbol{\varepsilon} = (\varepsilon_x, \varepsilon_y)$ the external laser field.

The power emitted by an accelerated electron is given by the Larmor formula:

$$\frac{dI(t)}{dt} = \frac{2e^2}{3c^3} |\boldsymbol{a}(t)|^2, \tag{8}$$

and the energy emitted in the energy range from ω to $\omega + d\omega$ is:

$$\frac{dI(\omega)}{d\omega} = \frac{4e^2}{3c^3} |\boldsymbol{a}(\omega)|^2, \tag{9}$$

where $\boldsymbol{a}(\omega)$ is the Fourier transform of the average electronic acceleration $\boldsymbol{a}(t) = d^2\boldsymbol{r}(t)/dt^2$ and $\boldsymbol{r}(t) = \langle \Psi(t)|\boldsymbol{r}|\Psi(t)\rangle$. The electric field emitted by the accelerated electron is:

$$\varepsilon_e = -\frac{e\{\hat{\boldsymbol{n}}(t) \times [\hat{\boldsymbol{n}}(t) \times \boldsymbol{a}(t)]\}}{r(t)c^2}, \tag{10}$$

https://doi.org/10.1017/S0263034616000914 Published online by Cambridge University Press

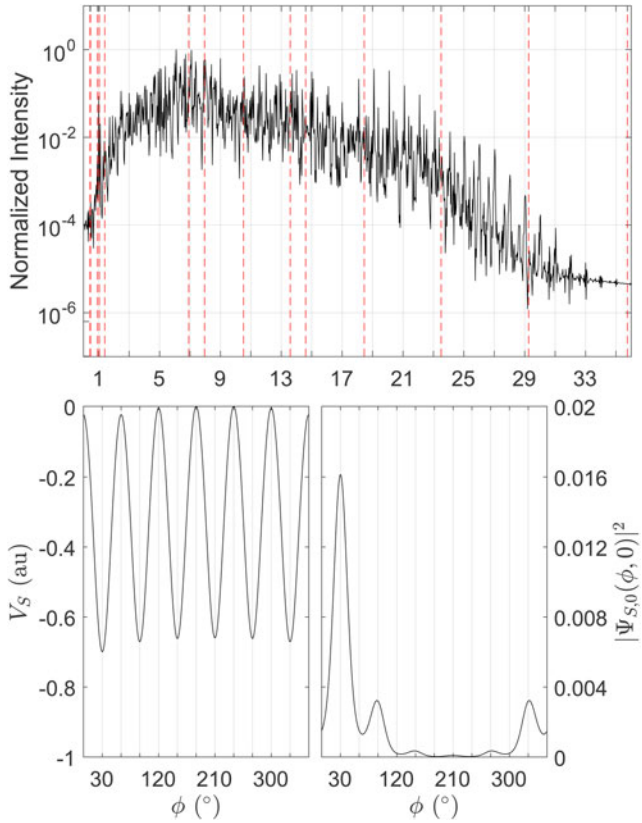

Fig. 5. Caption as Figure 1 but with $K_1 = 1.01K_0 = 1.9614$ au, which breaks the C6 symmetry.

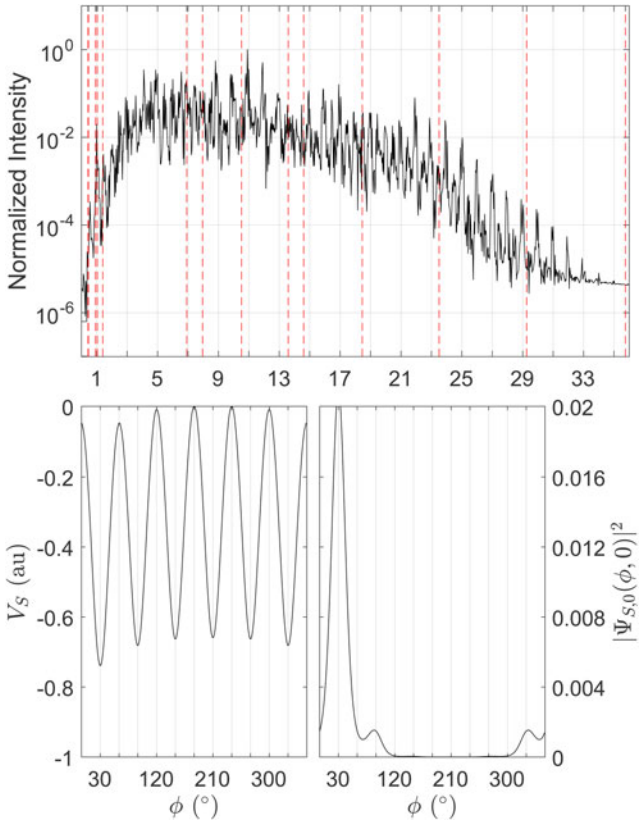

Fig. 6. Caption as Figure 1 but with $K_1 = 1.02K_0 = 1.9808$ au, which breaks the C6 symmetry.

where t is the retarded time, $\hat{\boldsymbol{n}}$ is the unit vector in the direction pointing from the position of the electron (at the retarded time t) to the observer; since $r(t) \gg R$, to consider $\hat{\boldsymbol{n}}$ pointing from the center of the ring is a fair assumption (Jackson, 1999).

A simple way to analyze the amplitudes and the phase of a plane monochromatic wave, defined in the Cartesian system, is to use the four Stokes parameters:

$$\begin{cases} S_0 = \varepsilon_{ex}^2(\omega) + \varepsilon_{ey}^2(\omega), \\ S_1 = \varepsilon_{ex}^2(\omega) - \varepsilon_{ey}^2(\omega), \\ S_2 = 2\varepsilon_{ex}(\omega)\varepsilon_{ey}(\omega)\cos(\delta), \\ S_3 = 2\varepsilon_{ex}(\omega)\varepsilon_{ey}(\omega)\sin(\delta), \end{cases} \tag{11}$$

$$S_0^2 = S_1^2 + S_2^2 + S_3^2, \tag{12}$$

where $\varepsilon_{ex}(\omega)$ and $\varepsilon_{ey}(\omega)$ are the Fourier transform of respectively $\varepsilon_{ex}(t)$ and $\varepsilon_{ey}(t)$; δ is the phase between the two fields (Born & Wolf, 2000). To characterize the polarization of the emission, introducing two independent quantities is expedient: the angle $(-\pi/4) \le \chi \le (\pi/4)$, which specifies the orientation of the polarization ellipse ($\tan\chi = \pm b/a$, where a and b are the major and the minor axes of the polarization ellipse) and the angle $0 \le \psi \le \pi$ between the polarization and the x-direction. We find:

$$S_1 = S_0 \cos 2\chi \cos 2\psi, \tag{13}$$

$$S_2 = S_0 \cos 2\chi \sin 2\psi, \tag{14}$$

$$S_3 = S_0 \sin 2\chi, \tag{15}$$

and thus for a monochromatic wave:

$$\tan 2\psi = \frac{S_2}{S_1} = \frac{2\varepsilon_{ex}(\omega)\varepsilon_{ey}(\omega)\cos(\delta)}{\varepsilon_{ex}^2(\omega) - \varepsilon_{ey}^2(\omega)}, \tag{16}$$

$$\begin{aligned} \tan 2\chi &= \frac{S_3}{\sqrt{S_1^2 + S_2^2}} \\ &= \frac{2\varepsilon_{ex}(\omega)\varepsilon_{ey}(\omega)\sin(\delta)}{\sqrt{(\varepsilon_{ex}(\omega) + \varepsilon_{ey}(\omega))^2 - 4\varepsilon_{ex}^2(\omega)\varepsilon_{ey}^2(\omega)\sin^2(\delta)}}. \end{aligned} \tag{17}$$

The spectrum obtained by the Fourier transform hides all information about the time dependence of the single harmonic; to get information on the temporal evolution of the emitted spectrum we resort to the Morlet transform of the

https://doi.org/10.1017/S0263034616000914 Published online by Cambridge University Press

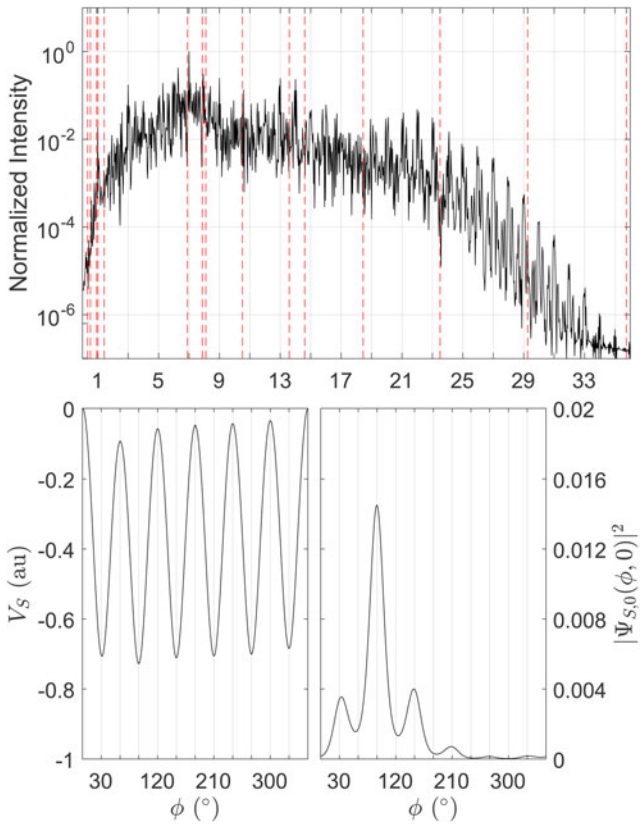

Fig. 7. Caption as Figure 1 but with $\phi_i = 30.75°$, 90°, 150°, 210°, 270°, 330°, which breaks the C6 symmetry.

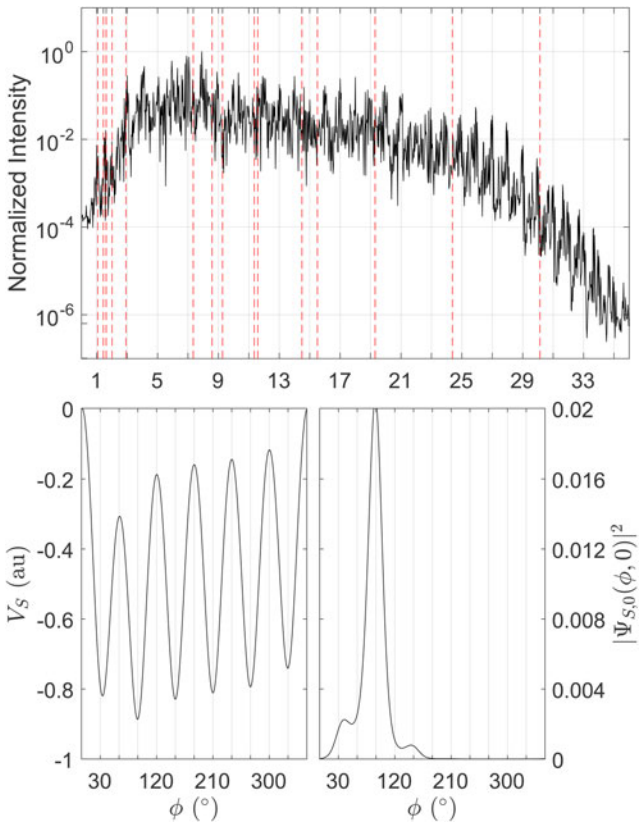

Fig. 8. Caption as Figure 1 but with $\phi_i = 32.5°$, 90°, 150°, 210°, 270°, 330°, which breaks the C6 symmetry.

acceleration, defined as

$$\begin{cases} \boldsymbol{a}(t_0;\omega) = \int_{-\infty}^{\infty} \boldsymbol{a}(t) M(t_0;\omega,t)dt, \\ M(t_0;\omega,t) = \sqrt{\omega}\left\{e^{-i[\omega(t-t_0)]} - e^{-\sigma_0^2/2}\right\} e^{-\omega^2(t-t_0)^2/(2\sigma_0^2)}, \end{cases} \tag{18}$$

where $\sigma_0 = 15$ is the number of oscillations at frequency ω within the Gaussian width and t_0 represents the time for which we require information (De Luca & Fiordilino, 1996; Chui, 2014) coherently with Eq. (9) we define Morlet power spectrum the quantity

$$\frac{\mathrm{d}I(t_0;\omega)}{\mathrm{d}\omega} = \frac{4e^2}{3c^3}|\boldsymbol{a}(t_0;\omega)|^2 \tag{19}$$

and assume that it gives the energy emitted in the frequency range ω, $\omega + d\omega$ at time t_0. As said before, to look not only for the total intensity of the radiation, but also for other important quantities in order to get important knobs for the improvement of new technology is of paramount importance. In this paper, we also look for the averaged emitted power in a time interval $\mathcal{T}$ as:

$$P(\mathcal{T}) = \frac{1}{\mathcal{T}}\int_{\mathcal{T}} \frac{dI(t)}{dt}dt. \tag{20}$$

3. RESULTS

In all simulations of this work we use a linearly polarized laser with $\phi_L = 60°$ (angle between the polarization axis and x-axis), wavelength $\lambda = 780$ nm, intensity $I_0 = 4 \times 10^{14}$ W/cm^2, and trapezoidal shape of 32 optical cycles (oc), ramping up and down for 3 oc. In the symmetrical case, $\mathbb{H}_S$ and $\mathbb{H}_C$ share the same symmetry, thus presenting the same degeneracy chain in their eigenstates, namely one non-degenerate state, two twofold-degenerate states, and one non-degenerate state. Moreover, always in the same case, with our choice of physical parameters the solutions of the time-independent Schrödinger equation for $\mathbb{H}_S$ are approximately equal to those for $\mathbb{H}_C$ given in (Castiglia *et al.*, 2015).

In Figure 1, we report, in the first row the Fourier spectrum for the symmetrical ring with the vertical dashed lines corresponding to the energy difference between the excited states and the ground state and, in the second row, V_S and the square modulus of the ground state of the Hamiltonian $\mathbb{H}_S$. Moreover, Figure 1 shows that $V_S \cong V_0 \cos 6\phi$ up to an additive constant when $V_0 = 0.33$ au. The spectrum contains

https://doi.org/10.1017/S0263034616000914 Published online by Cambridge University Press

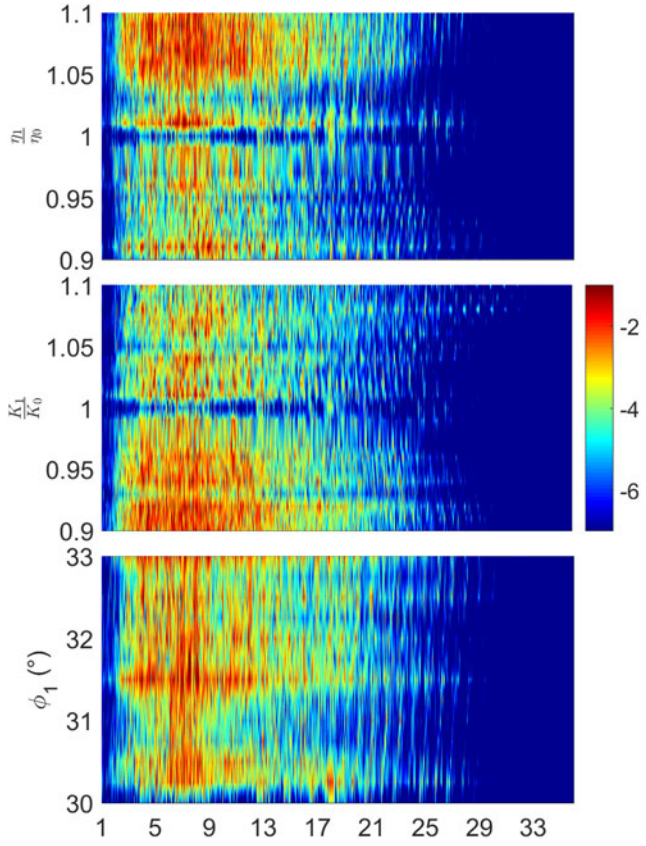

Fig. 9. First row: logarithm of Fourier spectrum versus harmonic order (in the *x*-axis) versus η_1 (in the *y*-axis) with $K_1 = K_0 = 1.9420$ au and $\phi_i = 30°, 90°, 150°, 210°, 270°, 330°$; second row: Fourier spectrum versus harmonic order (in the *x*-axis) versus K_1 (in the *y*-axis) with $\eta_1 = \eta_0 = 0.1333$ and $\phi_i = 30°, 90°, 150°, 210°, 270°, 330°$; third row: Fourier spectrum versus harmonic order (in the *x*-axis) versus ϕ_1 (in the *y*-axis) with $K_1 = K_0 = 1.9420$, $\eta_1 = \eta_0 = 0.1333$ and $\phi_{2,\ldots,6} = 90°, 150°, 210°, 270°, 330°$. The values of the parameters are: $V_0 = 0.33$ au, $R = 5$ au, $\lambda = 780$ nm, $I_0 = 4 \times 10^{14}$W/cm^2; the laser pulse has a trapezoidal shape (32 oc of full duration with 3 oc of up and down ramping) and is linearly polarized with $\phi_L = 60°$.

harmonic as well as non-harmonic lines, which could be used to synthesize short pulses.

As a second step, we wish to investigate the possibility of controlling the spectrum by introducing small modifications of V_S, thus we evaluate the dynamics of the system by varying η_1, K_1, and ϕ_1; we start by showing in Figures 2–4 the same quantities of Figure 1, respectively, for $\eta_1/\eta_0 = 0.97$, 0.99, and 1.03 (the other parameters are not modified). Owing to the reduced symmetry of the potential, the spectra now present both odd and even harmonics, but now the lines are less dense than in the spectrum of Figure 1; the spectrum in Figure 3 is well resolved (especially in the plateau region). However, the cutoff does not appear significantly changed; in agreement with Ref. (Castiglia *et al.*, 2015) the upper bound for the highest harmonic is:

$$\omega_c \cong \frac{2\varepsilon R}{\hbar}; \tag{21}$$

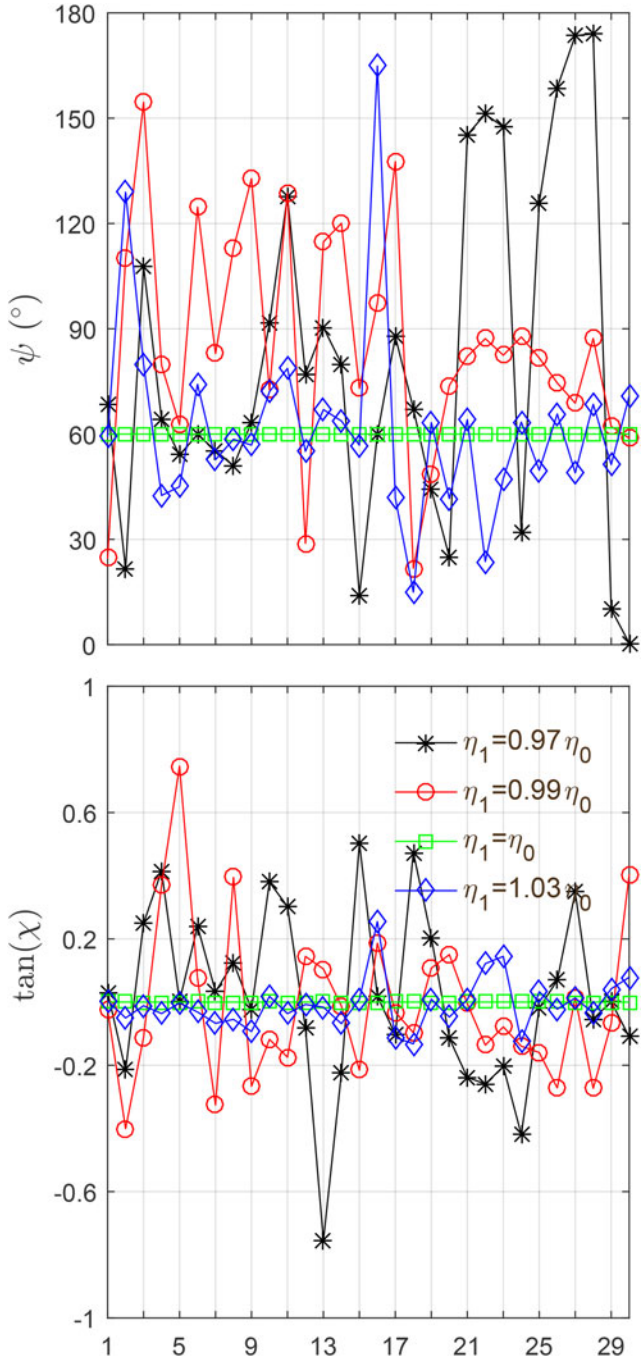

Fig. 10. First row: ψ versus harmonic order by varying η_1; second row: tanχ versus harmonic order by varying η_1. The values of the parameters are: $V_0 = 0.33$ au, $R = 5$ au, $K_1 = K_0 = 1.9420$ au, $\phi_i = 30°, 90°, 150°, 210°, 270°, 330°$, $\lambda = 780$ nm, $I_0 = 4 \times 10^{14}$W/cm^2, trapezoidal shape(32 oc, 3 up, and 3 down) linearly polarized with $\phi_L = 60°$.

by solving the canonical equations associated with the classical counterpart of $\mathbb{H}$ we find that the cutoff is $\omega_c \leq 2.8\varepsilon R/\hbar \cong 30\omega_L$ (Castiglia *et al.*, 2016). Attention must be paid to the physical meaning of setting different expressions for V_S. Obviously, by varying V_S we are changing the physical system and the differences are visible observing the ground states reported in Figures 2–4. Very small variations of the

https://doi.org/10.1017/S0263034616000914 Published online by Cambridge University Press

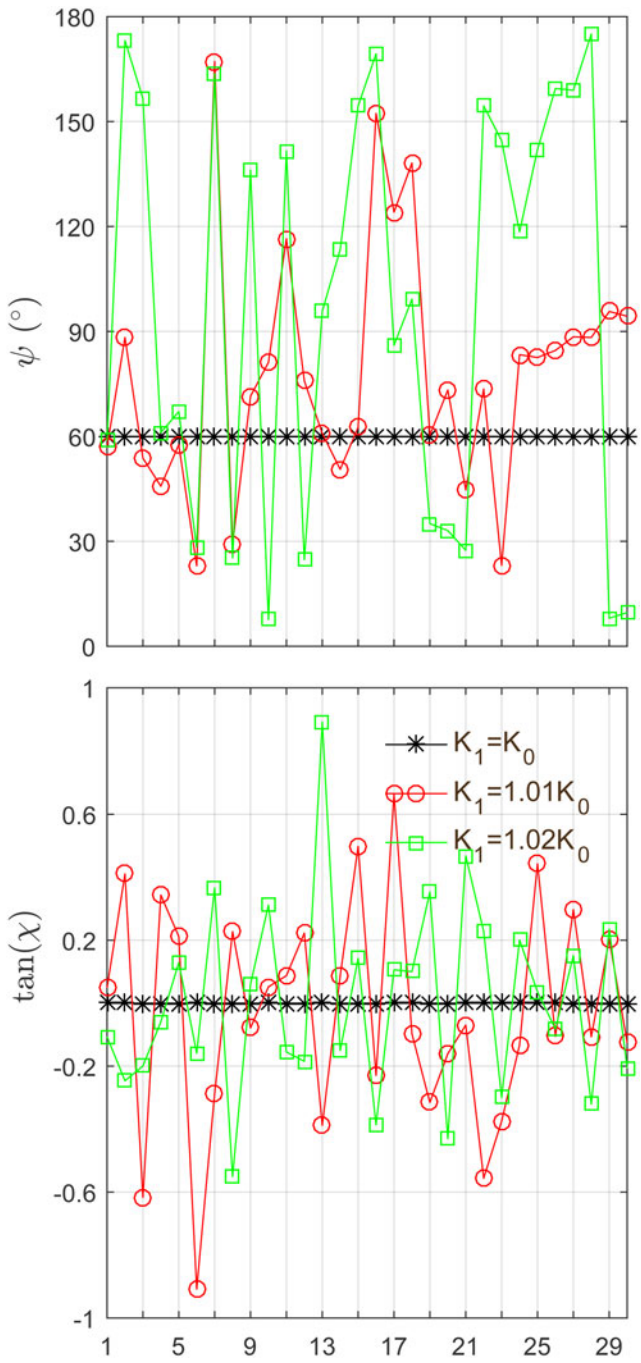

Fig. 11. First row: ψ versus harmonic order by varying K_1; second row: tanχ versus harmonic order by varying K_1. The values of the parameters are: V_0 = 0.33 au, R = 5 au, $\eta_1 = \eta_0$ = 1333, ϕ_i = 30°, 90°, 150°, 210°, 270°, 330°, λ = 780 nm, $I_0 = 4\times10^{14}$W/cm^2, trapezoidal shape(32 oc, 3 up, and 3 down) linearly polarized with ϕ_L = 60°.

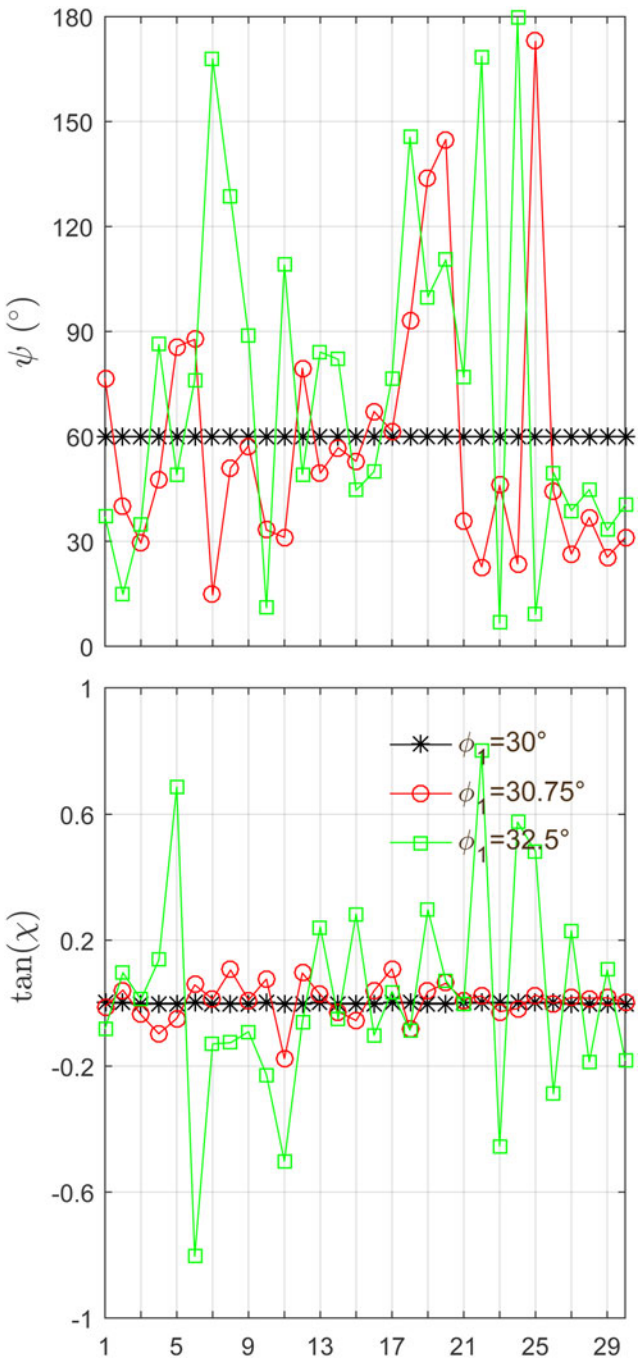

Fig. 12. First row: ψ versus harmonic order by varying ϕ_1; second row: tanχ versus harmonic order by varying ϕ_1. The values of the parameters are: V_0 = 0.33 au, R = 5 au, $\eta_1 = \eta_0$ = 1333, $K_1 = K_0$ = 1.9420 au, λ = 780 nm, $I_0 = 4\times10^{14}$W/cm^2, trapezoidal shape(32 oc, 3 up, and 3 down) linearly polarized with ϕ_L = 60°.

potential radically change the physical system, this is favorable to the goal of obtaining a tuning of the radiation properties, but the difference between the ground states can be used for better explaining some results. We note that Figure 4 ($\eta_1 = 1.03\eta_0$) presents a ground state closer to the symmetrical system of Figure 1 than the other cases; indeed we have significant variations in the ground state for $\eta_1 = 0.99\eta_0$ and a very different ground state for $\eta_1 = 0.97\eta_0$. Observing Figures 2 and 3 we note that both spectra present a rich plateau with only harmonic lines, but the first one is less resolved. At the same time, the ground state plots show that, with respect to the symmetrical case (Fig. 1), the population is mainly in the first dot, but in Figure 3 $|\Psi_S(30°, 0)|^2/|\Psi_S(90°, 0)|^2 \cong 3.5$ and in Figure 2 $|\Psi_S(30°, 0)|^2/|\Psi_S(90°, 0)|^2$

https://doi.org/10.1017/S0263034616000914 Published online by Cambridge University Press

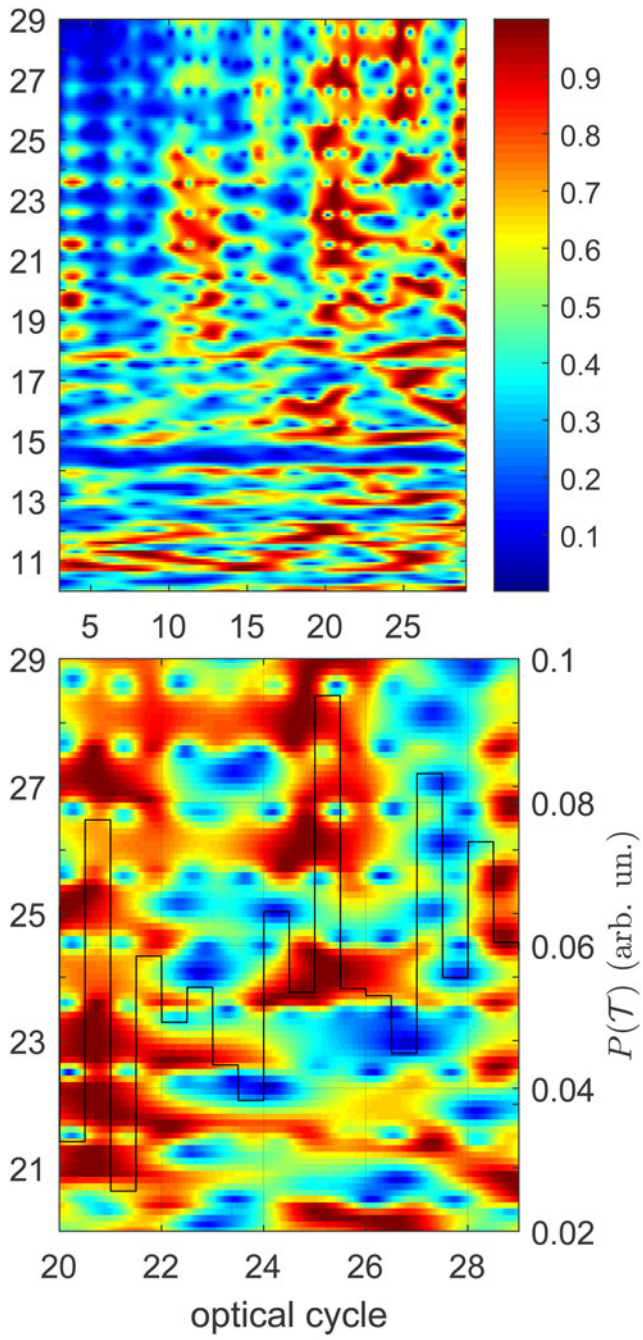

Fig. 13. First row: Morlet spectrum versus time in oc; second row: zoom of the Morlet spectrum and (in black histogram) $P(\mathcal{T})$ versus time in oc. The values of the parameters are: $V_0 = 0.33$ au, $R = 5$ au, $\eta_1 = 0.97\eta_0 = 0.1293$, $K_1 = K_0 = 1.9420$ au, $\phi_i = 30°, 90°, 150°, 210°, 270°, 330°$, $\lambda = 780$ nm, $I_0 = 4 \cdot 10^{14}\mathrm{W/cm^2}$, trapezoidal shape(32 oc, 3 up, and 3 down) linearly polarized with $\phi_L = 60°$.

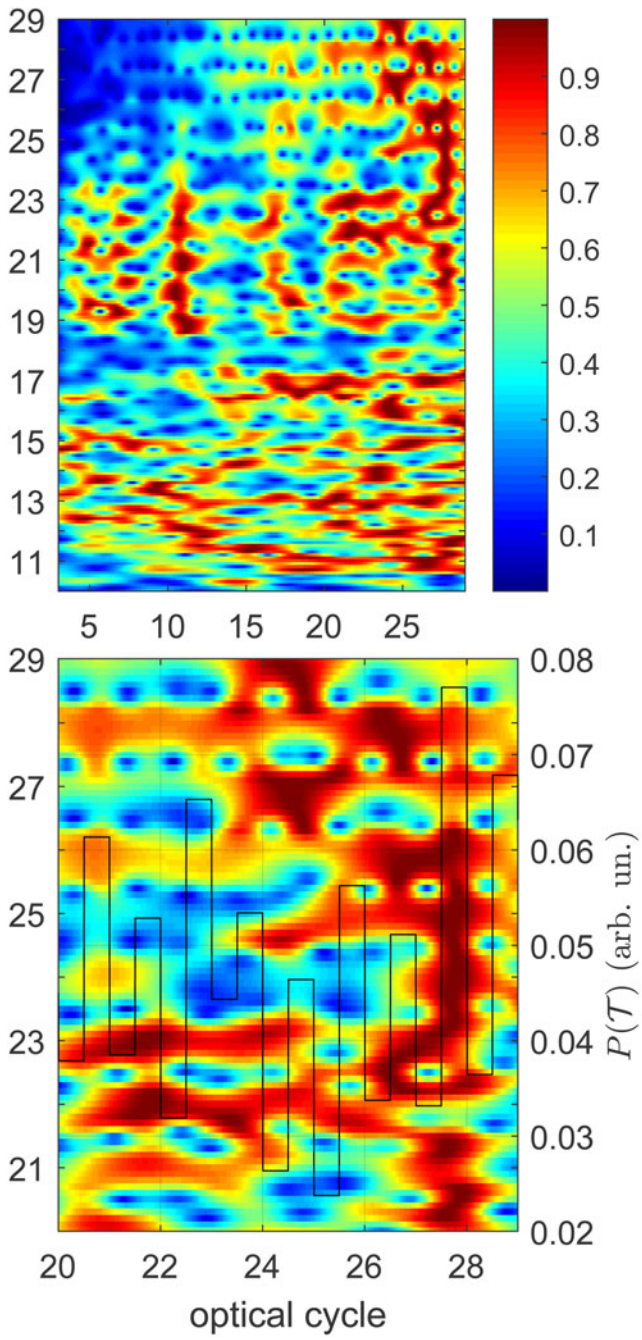

Fig. 14. First row: Morlet spectrum versus time in oc; second row: zoom of the Morlet spectrum and (in black histogram) $P(\mathcal{T})$ versus time in oc. The values of the parameters are: $V_0 = 0.33$ au, $R = 5$ au, $\eta_1 = 0.99\eta_0 = 0.1320$, $K_1 = K_0 = 1.9420$ au, $\phi_i = 30°, 90°, 150°, 210°, 270°, 330°$, $\lambda = 780$ nm, $I_0 = 4 \cdot 10^{14}\mathrm{W/cm^2}$trapezoidal shape (32 oc, 3 up, and 3 down) linearly polarized with $\phi_L = 60°$.

$\cong 22$; thus, the unbalance of population seems to play an important role.

In Figures 5 and 6, we show the results obtained for $K_1/K_0 = 1.01, 1.02$ (and the other parameters equal to the ones in Fig. 1); also in this case we could state that, by varying the ground state, the spectrum is, again, more resolved in harmonics, but if the ground state becomes very different with respect to the symmetrical case, the spectrum appears unresolved.

The previously analyzed two sets of systems present a specular symmetry for an axes passing along $\phi_1 = 30°$. In Figures 7 and 8, we break this symmetry by varying ϕ_1;

https://doi.org/10.1017/S0263034616000914 Published online by Cambridge University Press

with $\phi_1 = 32.5°$ (Fig. 8), we observe that the cutoff is considerably increased. Broad, resonant-like structures are present in all spectra (Figs 1–8); for example in Figure 1, around $7\omega_L$, $13\omega_L$, and $18\omega_L$; they are probably consequence of power broadened, Stark-shifted transitions.

In Figure 9, we make a systematic study of the cutoff, reporting the logarithm of the spectra by varying: in the first row η_1, in the second row K_1 and in the third ϕ_1. This analysis is important due to the fact that in the realization of short pulses by superposition of harmonic lines, it has been seen that the harmonics in the cut-off region may play a significant role (Krausz & Ivanov, 2009; Lu *et al.*, 2009). Although in Figure 9, there is not a clear behavior, to set parameters, in order to have a cutoff with six or seven harmonics more than in the symmetrical case, is possible. For example, we see an extended cutoff for $K_1 = 1.07K_0$, for $\eta_1 = 0.92\eta_0$, and for $\phi_1 = 32.5°$.

The study of the polarization of the emitted fields is reported in Figures 10–12, where we show the change of the ellipse of polarization for different values of, respectively, η_1, K_1, and ϕ_1. The polarization of the harmonics of the C_6 symmetrical system is the same of the incident laser, instead the other systems present harmonics polarized along different direction and with different ellipticity ($1 - b/a = 1 - \tan\chi$); it is interesting to note that, for small variations of the ground state $\eta_1 = 1.03\eta_0$, we have little variation of the polarization, on the other hand, for major variation we obtain very different ψ and χ.

To study the intensity of a particular harmonic at time t we evaluate the Morlet spectrum and we show it in Figures 13 and 14, respectively, for $\eta_1 = 0.97\eta_0$ and $0.99\eta_0$. In both configurations, we observe that the harmonics from 20th to 29th are emitted mainly in the same time intervals located after the 20th oc. In the bottom part of Figures 13 and 14, we plot the Morlet spectrum (color plot) and the averaged power $P(\mathcal{T})$ (in black histogram); the last is obtained by dividing the total observation time $32T_L$ in 64 equal intervals (thus every interval is of the type of $\mathcal{T}_n = [(n - 1/2)T_L, (n/2)T_L]$ with $n = 1, \ldots, 64$). This analysis allows us to see the correlation between the intensity of the averaged total power and the intensity of the highest-order harmonics. For example, observing the bottom part of Figure 13, we see that in the time interval [20.5, 21] oc the harmonics H21, H22, H23, H25, and H27 are emitted simultaneously and that $P(\mathcal{T})$ has a maximum. Thus, a strong intensity of the power is associated with a simultaneous emission of high-order harmonics.

4. CONCLUSION

In this paper, we look for the theoretical basis to design home-made nanosystems; in particular, we analyze the effect on the emission from different systems created by varying the potential felt by an electron. We have numerically studied a SQR driven by a strong laser field by varying its rotational symmetry, and we show that very small modifications of the system structure could give significant variation of the emitted spectrum. The fine tuning of the SQR is a method to set the properties of the home-made emitter. Another motivation to choose SQR comes from the very rich spectrum of the symmetrical case in Figure 1; this system is also a good choice because presents a high-intensity emission in the cut-off region that could be used to realize attosecond pulses, but also, by a fine tuning of the potential, it is possible to obtain other systems having only the harmonic lines. We point out that a system, without symmetry, presents both even and odd harmonics; see, for example, Figure 3. Actually an extension of the cutoff, but with a diminution of resolution, is also possible.

Analyzing the Stokes parameters, we see that within the same spectrum there are harmonics, in the far UV $\approx 39 \rightarrow 30$ nm (27th–20th harmonics), with different polarization. By opportune filtering, we reckon that it possible to isolate from the emitted spectrum a monochromatic radiation with required polarization.

In conclusion, we propose the realization of devices that permit the tuning of the radiation and in particular we analyze the potentiality of the SQRs that have very particular HHG spectrum. We show that with little changes of the symmetry of the system, to get different features in the HHG spectrum is possible and we suggest the manufacturing of similar system to obtain different nanodevices.

REFERENCES

Allaria, E., Callegari, C., Cocco, D., Fawley, W.M., Kiskinova, M., Masciovecchio, C. & Parmigiani, F. (2010). The FERMI@Elettra free-electron-laser source for coherent X-ray physics: photon properties, beam transport system and applications. *New J. Phys.* **12**, 075002.

Alon, O.E., Averbukh, V. & Moiseyev, N. (1998). Selection rules for the high harmonic generation spectra. *Phys. Rev. Lett.* **80**, 3743.

Antoine, P., L'Huillier, A. & Lewenstein, M. (1996). Attosecond pulse trains using high-order harmonics. *Phys. Rev. Lett.* **77**, 1234.

Baer, R., Neuhauser, D., Ždánská, P.R. & Moiseyev, N. (2003). Ionization and high-order harmonic generation in aligned benzene by a short intense circularly polarized laser pulse. *Phys. Rev. A* **68**, 043406.

Bâldea, I., Gupta, A.K., Cederbaum, L.S. & Moiseyev, N. (2004). High-harmonic generation by quantum-dot nanorings. *Phys. Rev. B* **69**, 245311.

Bauer, D. (1997). Two-dimensional, two-electron model atom in a laser pulse: Exact treatment, single-active-electron analysis, time-dependent density-functional theory, classical calculations, and nonsequential ionization. *Phys. Rev. A* **56**, 3028.

Born, M. & Wolf, E. (2000). *Principles of Optics: Electromagnetic Theory of Propagation, Interference and Diffraction of Light*. Cambridge: CUP.

Brandi, F., Neshev, D. & Ubachs, W. (2003). High-order harmonic generation yielding tunable extreme-ultraviolet radiation of high spectral purity. *Phys. Rev. Lett.* **91**, 163901.

Castiglia, G., Corso, P.P., Cricchio, D., De Giovannini, U., Frusteri, B. & Fiordilino, E. (2016). Classical chaos and harmonic

https://doi.org/10.1017/S0263034616000914 Published online by Cambridge University Press

generation in laser driven nanorings. *J. Phys. B – At. Mol. Opt.* **49**, 245601.

Castiglia, G., Corso, P.P., De Giovannini, U., Fiordilino, E. & Frusteri, B. (2015). Laser driven structured quantum rings. *J. Phys. B – At. Mol. Opt.* **48**, 115401.

Chang, Z. (2004). Single attosecond pulse and XUV supercontinuum in the high-order harmonic plateau. *Phys. Rev. A* **70**, 043802.

Chui, C.K. (2014). *An Introduction to Wavelets*, Vol. 1, Boston: Academic Press.

Ciappina, M.F., Becker, A. & Jaroń-Becker, A. (2008). High-order harmonic generation in fullerenes with icosahedral symmetry. *Phys. Rev. A* **78**, 063405.

Corkum, P.B. (1993). Plasma perspective on strong field multiphoton ionization. *Phys. Rev. Lett.* **71**, 1994.

Crawford-Uranga, A., De Giovannini, U., Räsänen, E., Oliveira, M.J.T., Mowbray, D.J., Nikolopoulos, G.M., Karamatskos, E.T., Markellos, D., Lambropoulos, P., Kurth, S. & Rubio, A. (2014). Time-dependent density-functional theory of strong-field ionization of atoms by soft X rays. *Phys. Rev. A* **90**, 033412.

Cricchio, D. & Fiordilino, E. (2014). Harmonic generation from nanorings driven by a two-color laser field. *Laser Phys. Lett.* **11**, 066002.

Cricchio, D. & Fiordilino, E. (2016). Wavelet analysis and HHG in nanorings: Their applications in logic gates and memory mass devices. *Nanoscale* **8**, 1968–1974.

Daniele, R., Castiglia, G., Corso, P.P., Fiordilino, E., Morales, F. & Orlando, G. (2009). Nuclear molecular dynamics investigated by using high-order harmonic generation spectra. *J. Mod. Opt.* **56**, 751–757.

Daniele, R. & Fiordilino, E. (1996). Bremsstrahlung and harmonic generation in laser-assisted electron–nucleus collision. *Nuovo Cimento D* **18**, 547–556.

De Luca, S. & Fiordilino, E. (1996). Wavelet temporal profile of high-order harmonics emitted by a two-level atom in the presence of a laser pulse. *J. Phys. B – At. Mol. Opt.* **29**, 3277–3292.

Di Piazza, A. & Fiordilino, E. (2001). Why hyper-Raman lines are absent in high-order harmonic generation. *Phys. Rev. A* **64**, 013802.

Eden, J.G. (2004). High-order harmonic generation and other intense optical field–matter interactions: review of recent experimental and theoretical advances. *Progr. Quantum Electron.* **28**, 197–246.

Farkas, G. & Tóth, C. (1992). Proposal for attosecond light pulse generation using laser induced multiple-harmonic conversion processes in rare gases. *Phys. Lett. A* **168**, 447–450.

Fiordilino, E., Morales, F., Castiglia, G., Corso, P.P., Daniele, R. & Strelkov, V.V. (2017). High-order harmonic generation via bound–bound transitions in an elliptically polarized laser field. *J. Opt. Soc. Am. B* **34**, 2673–2681.

Ganeev, R.A., Elouga Bom, L.B., Wong, M.C.H., Brichta, J.P., Bhardwaj, V.R., Redkin, P.V., & Ozaki, T. (2009). High-order harmonic generation from C_{60}-rich plasma. *Phys. Rev. A* **80**, 043808.

Ganeev, R., Suzuki, M., Baba, M., Kuroda, H. & Ozaki, T. (2005). High-order harmonic generation from boron plasma in the extreme-ultraviolet range. *Opt. Lett.* **30**, 768–770.

Ganeev, R.A., Witting, T., Hutchison, C., Frank, F., Redkin, P.V., Okell, W.A., Lei, D.Y., Roschuk, T., Maier, S.A., Marangos, J.P. & Tisch, J.W.G. (2012). Enhanced high-order-harmonic generation in a carbon ablation plume. *Phys. Rev. A* **85**, 015807.

Gavrila, M. (1992). *Atoms in Intense Laser Fields*. Boston: Academic Press.

Guo, Q., Kim, S.J., Kar, M., Shafarman, W.N., Birkmire, R.W., Stach, E.A., Agrawal, R. & Hillhouse, H.W. (2008). Development of $CuInSe_2$ nanocrystal and nanoring inks for low-cost solar cells. *Nano Lett.* **8**, 2982–2987.

Heinrich, A., Kornelis, W., Anscombe, M.P., Hauri, C.P., Schlup, P., Biegert, J. & Keller, U. (2006). Enhanced VUV-assisted high harmonic generation. *J. Phys. B – At. Mol. Opt.* **39**, S275.

Hinsche, N.F., Moskalenko, A.S. & Berakdar, J. (2009). High-order harmonic generation by a driven mesoscopic ring with a localized impurity. *Phys. Rev. A* **79**, 023822.

Hoffmann, M., Kärnbratt, J., Chang, M.H., Herz, L.M., Albinsson, B. & Anderson, H.L. (2008). Enhanced π conjugation around a porphyrin [6] nanoring. *Angew. Chem.* **120**, 5071–5074.

Jackson, J.D. (1999). *Classical Electrodynamics*. New York: Wiley.

Kouwenhoven, L.P., Austing, D.G. & Tarucha, S. (2001). Few-electron quantum dots. *Rep. Progr. Phys.* **64**, 701.

Krausz, F. & Ivanov, M. (2009). Attosecond physics. *Rev. Mod. Phys.* **81**, 163.

Lein, M. (2005). Attosecond probing of vibrational dynamics with high-harmonic generation. *Phys. Rev. Lett.* **94**, 053004.

Lewenstein, M., Balcou, P., Ivanov, M.Y., L'Huillier, A. & Corkum, P.B. (1994). Theory of high-harmonic generation by low-frequency laser fields. *Phys. Rev. A* **49**, 2117.

L'Huillier, A., Schafer, K.J. & Kulander, K.C. (1991). Theoretical aspects of intense field harmonic generation. *J. Phys. B – At. Mol. Opt.* **24**, 3315.

Lu, R.F., He, H.X., Guo, Y.H. & Han, K.L. (2009). Theoretical study of single attosecond pulse generation with a three-colour laser field. *J. Phys. B – At. Mol. Opt.* **42**, 225601.

Orlando, G., Castiglia, G., Corso, P.P. & Fiordilino, E. (2008). Bremsstrahlung from a repulsive potential: attosecond pulse generation. *J. Phys. B – At. Mol. Opt.* **41**, 055601.

Orlando, G., Corso, P.P., Fiordilino, E. & Persico, F. (2009*a*). Generation of isolated attosecond pulses using unipolar and laser fields. *J. Mod. Opt.* **56**, 1761–1767.

Orlando, G., Corso, P.P., Fiordilino, E. & Persico, F. (2009*b*). A three-colour scheme to generate isolated attosecond pulses. *J. Phys. B – At. Mol. Opt.* **43**, 025602.

O'Sullivan, M.C., Sprafke, J.K., Kondratuk, D.V., Rinfray, C., Claridge, T.D.W., Saywell, A., Blunt, M.O., O'Shea, J.N., Beton, P.H., Malfois, M., Anderson, H.L. (2011). Vernier templating and synthesis of a 12-porphyrin nano-ring. *Nature* **469**, 72–75.

Ozaki, T., Elouga Bom, L.B., Abdul-Hadi, J. & Ganeev, R. (2010). Evidence of strong contribution from neutral atoms in intense harmonic generation from nanoparticles. *Laser Part. Beams* **28**, 69–74.

Ozaki, T., Elouga Bom, L.B., Ganeev, R., Kieffer, J.C., Suzuki, M. & Kuroda, H. (2007). Intense harmonic generation from silver ablation. *Laser Part. Beams* **25**, 321–325.

Paul, P.M., Toma, E.S., Breger, P., Mullot, G., Augé, F., Balcou, P., Muller, H.G. & Agostini, P. (2001). Observation of a train of attosecond pulses from high harmonic generation. *Science* **292**, 1689–1692.

Rundquist, A., Durfee, C.G., Chang, Z., Herne, C., Backus, S., Murnane, M.M. & Kapteyn, H.C. (1998). Phase-matched generation of coherent soft X-rays. *Science* **280**, 1412–1415.

https://doi.org/10.1017/S0263034616000914 Published online by Cambridge University Press

Schafer, K.J., Yang, B., DiMauro, L.F. & Kulander, K.C. (1993). Above threshold ionization beyond the high harmonic cutoff. *Phys. Rev. Lett*. **70**, 1599.

Solanpää, J., Budagosky, J.A., Shvetsov-Shilovski, N.I., Castro, A., Rubio, A. & Räsänen, E. (2014). Optimal control of high-harmonic generation by intense few-cycle pulses. *Phys. Rev. A* **90**, 053402.

Strelkov, V. (2010). Role of autoionizing state in resonant high-order harmonic generation and attosecond pulse production. *Phys. Rev. Lett*. **104**, 123901.

van Kouwen, M.P., Reimer, M.E., Hidma, A.W., van Weert, M.H.M., Algra, R.E., Bakkers, E.P., Kouwenhoven, L.P. & Zwiller, V. (2010). Single electron charging in optically active nanowire quantum dots. *Nano Lett*. **10**, 1817–1822.

Wang, Z.L. (2004). Nanostructures of zinc oxide. *Mater. Today* **7**, 26–33.

Xie, X., Scrinzi, A., Wickenhauser, M., Baltuška, A., Barth, I. & Kitzler, M. (2008). Internal momentum state mapping using high harmonic radiation. *Phys. Rev. Lett*. **101**, 033901.

Zepf, M., Dromey, B., Landreman, M., Foster, P. & Hooker, S.M. (2007). Bright quasi-phase-matched soft-x-ray harmonic radiation from argon ions. *Phys. Rev. Lett*. **99**, 143901.

Zhukovsky, K. (2016). Emission and tuning of harmonics in a planar two-frequency undulator with account for broadening. *Laser Part. Beams* **34**, 447–456.

Zuo, T., Bandrauk, A.D., Ivanov, M. & Corkum, P.B. (1995). Control of high-order harmonic generation in strong laser fields. *Phys. Rev. A* **51**, 3991.